Formation of Segregation Morphology in Crystalline/Amorphous Polymer Blends: Molecular Weight Effect

Hsin-Lung Chen,*,† Lain-Jong Li,† and Tsang-Lang Lin‡

Department of Chemical Engineering, and Department of Engineering and System Science, National Tsing Hua University, Hsin-Chu, Taiwan, 30043, R.O.C

Received October 27, 1997; Revised Manuscript Received January 25, 1998

ABSTRACT: In a melt-miscible crystalline/amorphous polymer blend, crystallization is accompanied with the segregation of amorphous diluent. Depending on the distance of segregation, various types of segregation morphology, including interlamellar, interfibrillar, and interspherulitic, may be created. In this study, we systematically investigated the effects of molecular weight (MW) of both crystalline and amorphous component on the formation of segregation morphology in polycaprolactone (PCL)/poly(vinyl chloride) (PVC) blends. Optical microscopy and small-angle X-ray scattering (SAXS) revealed that the extent of interfibrillar morphology increased with decreasing MW of PCL (M_{PCL}). However, in the blends containing oligomeric PCL, interfibrillar segregation also involved the exclusion of uncrystallizable PCL short chains. The volume fraction of PVC expelled into the interfibrillar regions was calculated from SAXS linear crystallinity and bulk crystallinity. The results indicated that the transport of PVC into interfibrillar regions was facilitated by decreasing M_{PCL} for PCL/PVC 80/20 blend. However, the extent of PVC expelled interfibrillarly was relatively unaffected by M_{PCL} for the 70/30 and 60/40 blends. The variation of crystal growth rate with M_{PCL} played a key role in controlling the segregation distance of PVC. Increasing the molecular weight of PVC (M_{PVC}) was found to shorten the segregation distance. The dependence of growth rate on M_{PVC} again governed the length scale of PVC segregation.

Introduction

Polymer blends containing crystallizable components have gained significant interests because of the rich morphology offered by these systems. In a melt-miscible crystalline/amorphous blend, crystallization must involve the segregation of amorphous diluent. Depending on the distance of segregation, various types of morphology may be created; this includes (1) interlamellar segregation, where segregation of diluent occurs at lamellar level, so that the diluent is located in the interlamellar regions; (2) interfibrillar segregation, where the diluent is segregated by a larger distance to the regions between the lamellar bundles in spherulites; (3) interspherulitic segregation, where the diluent is segregated by the largest distance to the regions between spherulites.[1] A blend system does not necessarily display only one type of morphology. Different types of morphology may coexist, leading to multiple locations for the amorphous diluent.[2−6]

Segregation of amorphous diluent is natural since the driving force of crystallization tends to separate the two components from being mixed. However, the principle dictating the location of diluent is not well understood. It has been suggested that the diluent molecules confined in the interlamellar regions are deformed by the crystals and have lower conformational entropy. An entropic driving force is thus developed, tending to pull the diluent molecules out of the interlamellar regions.[7] In addition to this entropic force, we suggest that the crystallization driving force of the crystallizable segments within the interlamellar zones should act as another force to push the diluent out of the interlamellar regions. Two driving forces then exist to reject the amorphous diluent out of the interlamellar zones: namely, the entropic force associated with the tendency to resume random-coiled conformation and the crystallization driving force of crystallizable segments in the interlamellar regions. These two forces compete against the favorable interaction between the diluent and the amorphous portion of the crystalline polymer in the interlamellar regions. Exclusion of amorphous diluent out of the interlamellar regions is consequently governed by the magnitude of interaction (χ parameter), the interlamellar distance (which determines the extent that the diluent molecules are deformed), and the degree of supercooling (which determines the driving force of crystallization). All of these may depend on composition, temperature, and molecular weight.

The above discussion is based purely on thermodynamic ground. Even if the two forces associated with extralamellar segregation can supersede the favorable interaction, extralamellar placement of diluent is not guaranteed. Kinetically, chain diffusivity may also be an important factor. Keith and Padden suggested that the distance over which uncrystallizable impurity may be segregated is determined by the interplay between the diffusion coefficient (D) of impurity molecules and the crystal growth rate (G). If the diffusion rate of diluent is relatively slower than the crystal growth rate, diluent molecules may be trapped inside the interlamellar regions before they had a chance to diffuse out. The interplay between D and G is defined by the parameter, $\delta = D/G$.[8] δ has the unit of length and thus provides a qualitative measure of segregation distance. Likewise, δ may depend on composition, temperature, and molecular weight.

Extensive studies have been conducted to evaluate the segregation morphology for various blends (e.g. refs 2−7 and 9−18). Most works have focused on revealing the morphology in specific systems, while limited attempts

* Author to whom correspondence should be addressed.
† Department of Chemical Engineering.
‡ Department of Engineering and System Science.

S0024-9297(97)01574-X CCC: $15.00
Published on Web 03/12/1998

Table 1. Molecular Weights of PCL and PVC Samples Used in This Study

sample	M_n	M_w
PCL1	800	1100
PCL2	1100	2400
PCL3	1200	2600
PCL4	7500	9800
PCL5	15800	33800
PCL6	34800	48700
PCL7	43700	62400
PVC1	7200	15000
PVC2	25500	42400
PVC3	32400	50300
PVC4	39800	60200
PVC5	59700	74700

have been made to systematically evaluate the variables that could affect the formation of segregation morphology. Groeninckx et al. studied the effect of diluent T_g on the segregation distance in polycaprolactone (PCL)/poly(vinyl chloride) (PVC) and PCL/chlorinated polyethylene (CPE) blends. Using CPE with the same chlorine content as PVC (56.3 wt %), PCL/CPE blends were found to exhibit a longer segregation distance than PCL/PVC. The lower T_g of CPE was suggested to give rise to the longer segregation distance. Recently, Runt et al. considered the roles of both intermolecular interaction and diluent T_g on the segregation distance.[18] They concluded that for weakly interacting systems, diluent T_g governs the length scale of segregation. However, diluent T_g no longer plays a decisive factor for strongly interacting systems. The presence of strong interactions helps to promote the segregation distance by depressing the crystal growth rate. The crystal growth rate, and hence the factors that influence it, was suggested to dominate the length scale of diluent segregation.[18]

Molecular weights (MW) of both crystalline and amorphous components are another important variable because they may influence both the kinetic and thermodynamic parameters governing the segregation distance. To our knowledge, no systematic study has been conducted to evaluate MW effect on the length scale of diluent segregation in polymer blends. In a previous study, we have prepared PCL samples with a wide range of MW ($M_n \approx 1900-64700$) through fractionation via simple precipitation.[19] These materials should be useful for studying the effect of crystalline component MW on the segregation behavior in PCL/PVC blends. In addition, we also prepared a series of PVC samples with M_n ranging from 7200 to 59 700 for evaluating the effect of diluent MW on the length scale of segregation. In this article, the influence of MW on the segregation distance in PCL/PVC blends is reported. The length scales of segregation corresponding to different MW are characterized by optical microscopy and small-angle X-ray scattering (SAXS). The MW−crystal growth rate−segregation distance relationship will be critically discussed in this paper.

Experimental Section

Materials and Sample Preparation. PCL with various MW were prepared in the previous study.[19] The MW of PCL samples used are tabulated in Table 1. PVC samples with MW ranging from $M_n \approx 7200-59700$ were also prepared following a similar procedure for preparing the PCL samples. Two as-received PVCs acquired from Formosa Plastics Co. Ltd., Taiwan, and Aldrich were used as the starting materials for MW fractionation. Table 1 also lists the MW of PVC used in this study. The values of MW reported are absolute MW measured by a Kratos Model Spectraflow 400 Gel Permeation Chromatography (GPC) equipped with Shodex KF-801, KF-802, KF-803, and KF-804 columns and Viscotek Model-100 differential refractometer/viscometer detectors. The average molecular weights (M_n and M_w) were obtained through the universal calibration curve using the Viscotek Unical GPC software, version 4.01.

Blendings of PCL with PVC were carried out by solution casting. The blending components were dissolved in tetrahydrofuran (THF) at room temperature yielding a 1 wt % solution. The solution was subsequently poured onto a Petri dish and the blend film was obtained after evaporating most THF solvent on a hot plate at ca. 60 °C. The blend film was further dried in vacuo at 60 °C for 24 h.

Samples for SAXS study were prepared by compression molding. The blend obtained from solution casting was compression molded by a hot press at 100 °C for 10 min to yield a disk of ca. 1 mm thick. The sample was then quickly transferred into an oven equilibrated at 30 °C for crystallization. Since the SAXS analysis presented in this study requires the spherulites within the sample to be volume filling, crystallization at 30 °C was conducted for 96 h. Optical microscopy confirmed that volume-filling spherulites were obtained through such a crystallization condition.

Differential Scanning Calorimetry and Polarized Optical Microscopy. Bulk crystallinities of PCL/PVC blends were measured by a TA Instrument 2000 differential scanning calorimeter (DSC). The samples used for DSC measurement were cut directly from the sample disks for SAXS measurement. Crystallinity was calculated from the enthalpy of melting. The degree of crystallinity measured by DSC corresponds to the weight fraction of crystals (w_c). Weight fraction was converted to volume fraction (ϕ_c) using a formula derived by Runt et al.[18]

The spherulite morphology and growth rate were monitored with an Olympus BH-651P polarized optical microscope. The sample was first melted on a Linkam HFS91 hot stage at 100 °C for 3 min. The sample was then quickly transferred to another hot stage equilibrated at 30 °C and the spherulite growth was monitored. Micrographs were taken at intervals for measuring the spherulite radii (R) at various time periods. The growth rate was calculated from the change of spherulite radius with time, dR/dt.

SAXS Measurement. All SAXS measurements were performed at room temperature. The X-ray source was operated at 200 mA and 40 kV. The X-ray source is a 18 kW rotating anode X-ray generator (Rigaku) equipped with a rotating anode Cu target. The incident X-ray beam was monochromated by a pyrolytic graphite and a set of three pinhole inherent collimators were used so that the smearing effects inherent in slit-collimated small-angle X-ray cameras can be avoided. The sizes of the first and second pinhole are 1.5 and 1.0 mm respectively, and the size of the guard pinhole before the sample is 2.0 mm. The scattered intensity was detected by a two-dimensional position sensitive detector (ORDELA Model 2201X, Oak Ridge Detector Laboratory Inc.) with 256 × 256 channels (active area 20 × 20 cm^2 with ~1 mm resolution). The sample to detector distance is 4000 mm long. The beam stop is around lead disk of 18 mm in diameter. All data were corrected by the background (dark current and empty beam scattering) and the sensitivity of each pixel of the area detector. The area scattering pattern has been radially averaged to increase the efficiency of data collection compared with one-dimensional linear detector. Data were acquired and processed on an IBM-compatible personal computer.

SAXS Data Analysis. In this study, the morphological parameters, including long period (L), crystal thickness (l_c), and amorphous layer thickness (l_a), were determined by SAXS. Two approaches may be utilized for obtaining these parameters. i.e., one-dimensional correlation function and interphase distribution function. From the scattering intensity ($I(q)$)

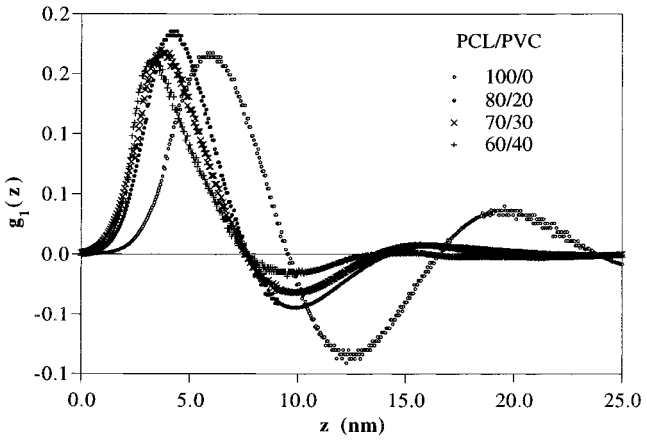

Figure 1. Representatives of interphase distribution function of PCL/PVC blends. The MW of PCL and PVC are 34 800 and 39 800, respectively. The blend compositions are indicated in the figure.

profile, the one-dimensional correlation function is defined as[20]

$$\gamma(z) = \frac{1}{\gamma(0)}\int_0^\infty I(q)q^2 \cos(qz)\, dq \tag{1}$$

where $q = 4\pi/\lambda \sin(\theta/2)$ (θ = scattering angle) and z is the direction along which the electron density is measured. $\gamma(0)$ is just the scattering invariant:

$$Q = \int_0^\infty Iq^2\, dq \tag{2}$$

Therefore, the correlation function defined by eq 1 has been normalized by the invariant.

Since the experimentally accessible q range is finite, extrapolation of intensity to both low and high q is necessary. Extrapolation to zero q is accomplished by the Debye-Bueche model[21−22]

$$I(q) = \frac{A}{(1 + a_c^2 q^2)^2} \tag{3}$$

where A is a constant and a_c is the correlation length. A and a_c can be determined from the plot $I(q)^{-1/2}$ vs q^2 using the intensity data at low q region (0.11 nm^{-1} to 0.16 nm^{-1} in this study). Extension to large q can be performed using the Porod-Ruland model[23]

$$I(q) = K_p \frac{\exp(-\sigma^2 q^2)}{q^4} + I_{fl} \tag{4}$$

where K_p is the Porod constant, σ is a parameter related to the thickness of crystal/amorphous interphase, and I_{fl} is the background intensity arising from thermal density fluctuation. The values of K_p, σ, and I_{fl} were obtained by curve fitting the intensity profile at large q region (1.1−1.3 nm^{-1}).

Determinations of l_c, l_a, and L may be realized by locating the first minimum and maximum in the one-dimensional correlation function.[20] However, a recent study by Santa Cruz et al. showed that the positions of minimum and maximum in the correlation function may be perturbed by the broad size distribution of lamellae.[24] It was suggested that l_c, l_a, and L can be more reliably determined from the interphase distribution function, $g_1(z)$, which is given by the second derivative of $\gamma(z)$:[24−25]

$$g_1(z) = \gamma''(z) \tag{5}$$

Representatives of $g_1(z)$ of PCL/PVC blends are displayed in Figure 1. Assuming an ideal two-phase system with sharp phase boundary, the interphase distribution function is a

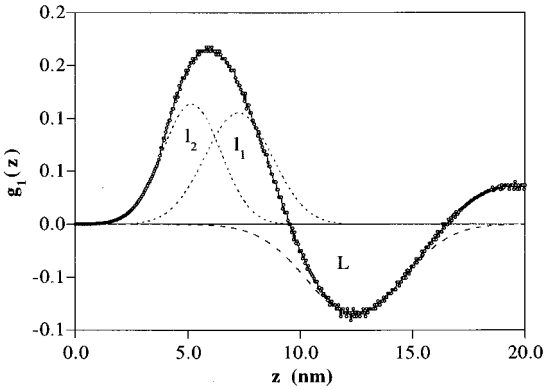

Figure 2. Deconvolution of interphase distribution function showing two positive peaks (l_2 and l_1) associated with the distribution of crystal and amorphous layer and a negative peak (L) associated with the distribution of a long period. The curve fit was performed assuming Gaussian distribution of l_1, l_2, and L.

superposition of three contributions, namely, two positive peaks associated with the size distributions of crystalline and amorphous layers and a negative peak due to the distribution of long period.[24] Curve fits may be performed to deconvolute these contributions. In this study, curve fit was evaluated by assuming Gaussian distributions of l_c, l_a, and L.[24] Figure 2 illustrates the deconvolution of $g_1(z)$.

From the interphase distribution function, it is not possible to distinguish which one of the two positive peaks corresponds to l_c and which one to l_a. Following the notation of Santa Cruz et al., we denote the smaller length (the first peak) l_2 and the larger one (the second peak) l_1. When the linear crystallinity, ϕ_c^{lin}, is smaller than 0.5, l_1 is l_c and l_2 corresponds to l_a. The inverse is true for $\phi_c^{lin} > 0.5$. Linear crystallinity is defined as

$$\phi_c^{lin} = \frac{l_c}{L} = \frac{l_c}{l_c + l_a} \tag{6}$$

Provided that spherulites are volume filling, ϕ_c^{lin} is related to the bulk crystallinity, ϕ_c (i.e. the crystallinity measured by density or thermal analysis) by

$$\phi_c = \phi_s \phi_c^{lin} \tag{7}$$

where $\phi_s = \phi_c/\phi_c^{lin}$, the volume fraction of lamellar stacks in the sample. If the whole volume is filled with lamellar stacks, $\phi_s = 1$ and $\phi_c^{lin} = \phi_c$; if the sample is not homogeneously filled with lamellar stacks (such as the case of the interfibrillar morphology), $\phi_s < 1$ and $\phi_c^{lin} > \phi_c$.

For PCL/PVC blends containing more than 20 wt % PVC, ϕ_c is easily below 0.5 (for example, ϕ_c of 70/30 blend is around 0.3), it is reasonable to assign $l_1 = l_a$ and $l_2 = l_c$ for these compositions. For pure PCL and the 80/20 blend containing oligomeric PCL, ϕ_c is close to 0.5, and the assignment became less straightforward. In these cases, assignments of l_1 and l_2 were justified from the values of ϕ_s. For pure PCL with MW (M_{PCL}) = 1200 and 15 800 (ϕ_c = 0.58 and 0.52, respectively), if l_1 were assigned as l_a, then ϕ_s of these two samples would be 1.33 and 1.24, respectively, which are meaningless. Alternatively, l_1 was assigned as l_c, and the values of ϕ_s were found to assume reasonable values of 1.00 and 0.90, respectively. For the other two pure PCL with high MW (M_{PCL} = 34 800 and 43 700), l_1 was assigned as l_a, and the value of ϕ_s thus obtained was very close 1.0.

For 80/20 blend containing oligomeric PCL (M_{PCL} = 800 and 1200), ϕ_c is around 0.43. From polarized optical microscopy, we found that blends with lower M_{PCL} displayed clearer interfibrillar morphology (as will be shown in Figure 3 in the **Results and Discussion**). This means ϕ_s must drop with decreasing M_{PCL}. If l_2 were taken as l_c for the 80/20 blend

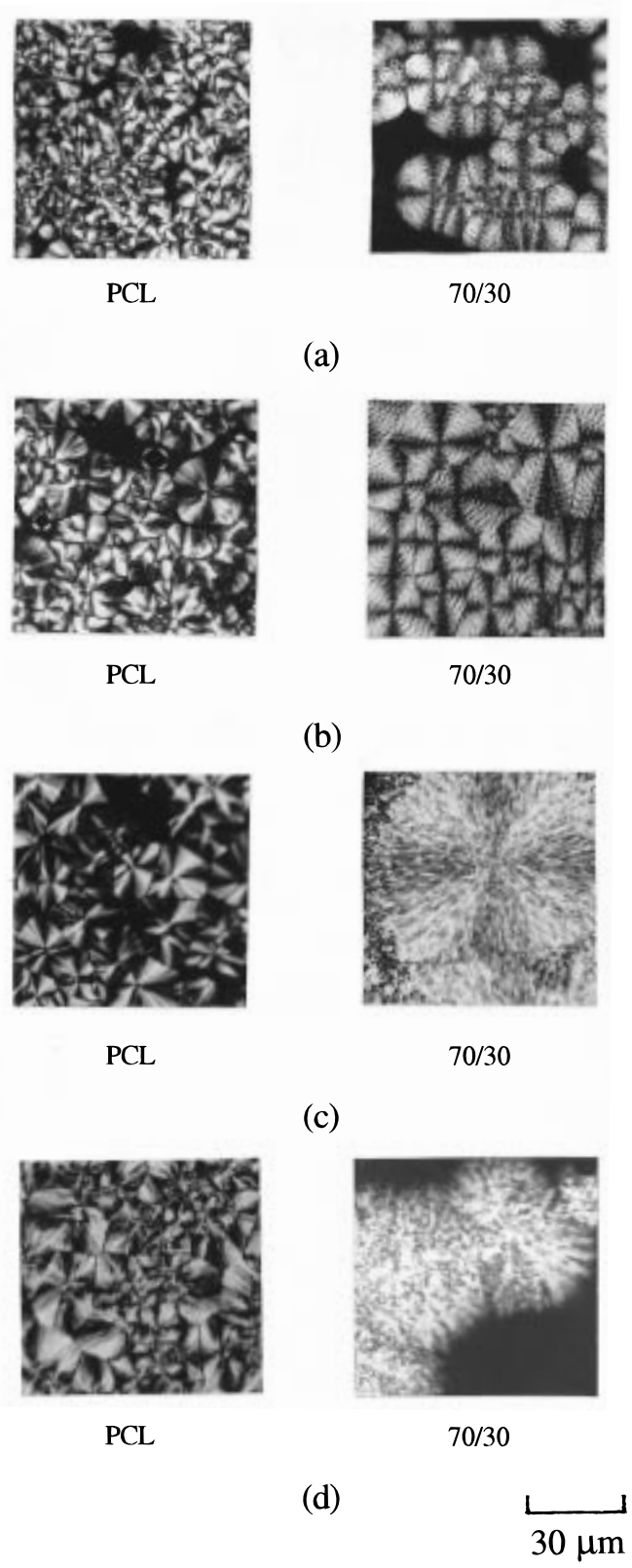

Figure 3. Spherulite morphologies of PCL and corresponding PCL/PVC 70/30 blends with various M_{PCL}. MW of PVC was fixed as M_n = 39 800. The MW of PCL: (a) 34 800; (b) 15 800; (c) 7500; (d) 1200.

containing oligomeric PCL, such a trend was not identified, but instead, a higher value of ϕ_s was obtained for the oligomeric blend. The assignment was hence exchanged, and the expected trend was identified. Table 2 tabulates the values of ϕ_s. For pure PCL, ϕ_s is close to unity. For the three blend compositions, ϕ_s is found to drop with decreasing M_{PCL}, which is consistent with the microscopic observation. Details will be discussed later.

Table 2. Linear Crystallinity (ϕ_c^{Lin}), Bulk Crystallinity (ϕ_c), and Volume Fraction of Lamellar Stacks (ϕ_s) of PCL/PVC Blends with Different M_{PCL}

PCL/PVC composition	M_{PCL}[a]	ϕ_c^{lin}	ϕ_c	$\phi_s = \phi_c/\phi_c^{lin}$ [b]
100/0	1200	0.57	0.58	1.02 (≈1.0)
	15800	0.58	0.52	0.90
	34800	0.42	0.42	1.00
	43700	0.42	0.43	1.02 (≈1.0)
80/20	800	0.58	0.43	0.74
	1200	0.58	0.42	0.72
	15800	0.39	0.39	1.00
	34800	0.40	0.36	0.90
70/30	1100	0.41	0.29	0.71
	1200	0.44	0.31	0.70
	15800	0.43	0.33	0.77
	34800	0.38	0.30	0.79
60/40	800	0.39	0.22	0.56
	1200	0.39	0.26	0.67
	7500	0.38	0.28	0.74
	15800	0.40	0.32	0.80
	34800	0.39	0.30	0.77

[a] M_{PCL} signifies the M_n of PCL. [b] The error associated with ϕ_s is ±0.02

Results and Discussion

1. Effect of PCL Molecular Weight. In discussing the effect of M_{PCL} on segregation morphology, M_{PCL} is the variable and the MW of PVC (M_{PVC}) is fixed as 39800. M_{PCL} and M_{PVC} signify M_n of the corresponding polymer. The crystallization temperature is 30 °C.

(A) Microscopic Observation and SAXS Morphological Parameters. Figure 3 displays the spherulite morphologies of pure PCL and corresponding PCL/PVC 70/30 blend with different M_{PCL}. For the two samples with high M_{PCL} (M_n = 15 800 and 34 800), spherulites in the blends exhibit banded patterns. Compared with the smooth spherulite texture of the corresponding pure PCL, these spherulites are coarser and consist of lamellar bundles of larger cross section. This coarseness may be caused by the exclusion of uncrystallizable materials from the lamellar bundles and subsequently resides in the interfibrillar regions.[26] The spherulites become more open with decreasing M_{PCL}, and this is particularly evident for the blends containing oligomeric PCL. The exclusion of uncrystallizable materials into interfibrillar regions appears to be promoted by lowering the MW of PCL.

The morphological feature is further revealed by SAXS study. Figure 4a shows the profiles of Lorentz-corrected intensity (Iq^2) for the blends with M_{PCL} = 34 800. The value of q at which the intensity maximum is located (q_{max}) increases with PVC composition, implying that the long period calculated from Bragg's law is reduced upon blending. This observation is different from the previous study showing increasing long period with PVC composition.[9] Figure 4b plots the morphological parameters as a function of the weight fraction of PVC (w_{PVC}) for the blends with M_{PCL} = 34 800. L, l_c, and l_a all drop with w_{PVC}; similar composition variations are identified for blends with other M_{PCL}.

Shown in Figure 5a are the profiles of Lorentz-corrected intensity for 70/30 blends with different M_{PCL}. q_{max} is relatively independent of M_{PCL}. Figure 5b displays the dependences of l_c, l_a, and L on M_{PCL} for the 60/40 blend. The crystal thickness is about constant

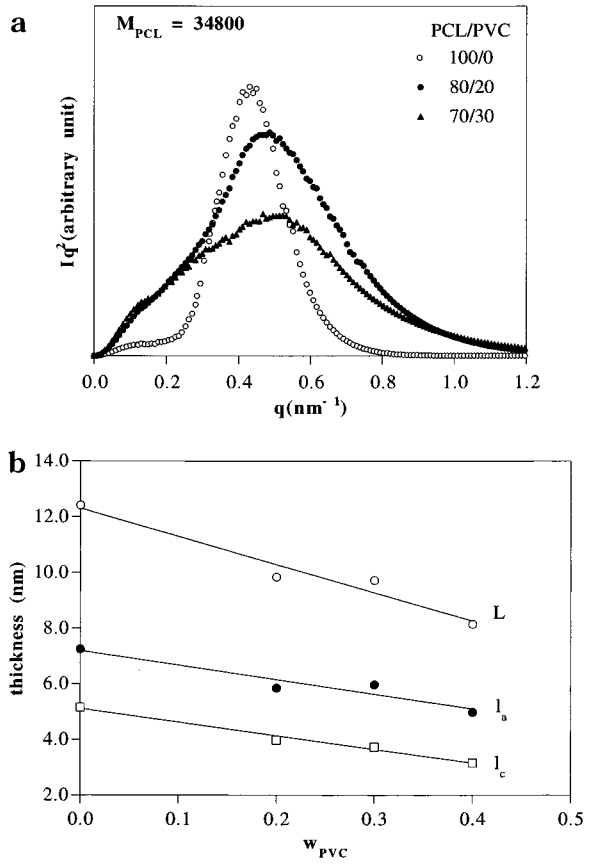

Figure 4. (a) Profiles of Lorentz-corrected intensity of PCL/PVC blends with M_{PCL} = 34 800. (b) Variations of SAXS long period (L), crystal thickness (l_c), and amorphous layer thickness (l_a) with PVC composition for PCL/PVC blends (M_{PCL} = 34 800).

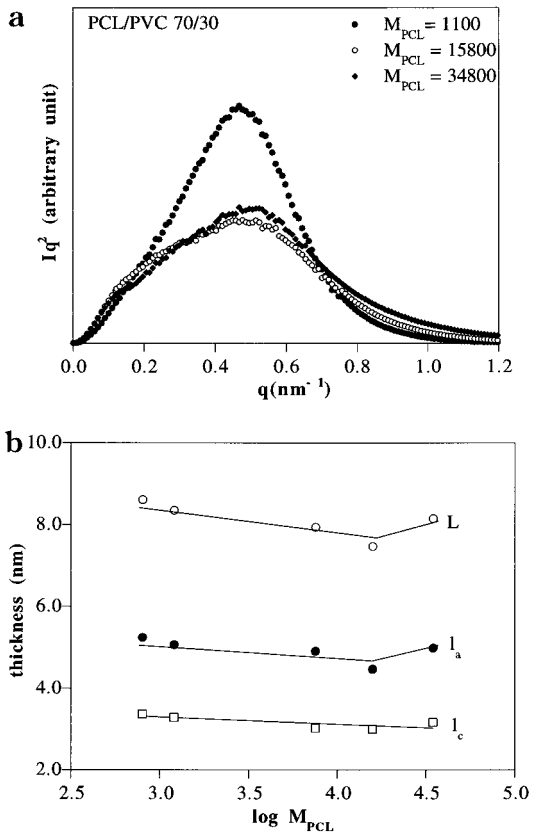

Figure 5. (a) Profiles of Lorentz-corrected intensity of PCL/PVC 70/30 blend with different M_{PCL}. (b) Variations of L, l_c, and l_a with M_{PCL} for PCL/PVC 60/40 blend.

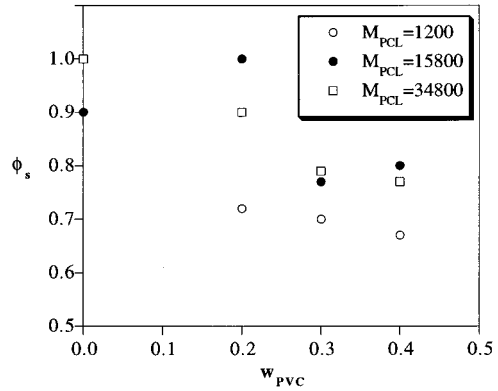

Figure 6. Variation of the volume fraction of lamellar stacks (ϕ_s) with PVC composition. Symbols corresponding to different M_{PCL} are indicated in the figure.

while l_a and L rise slightly (by less than 1 nm) with increasing M_{PCL} at the high MW regime.

(B) Identification of Segregation Morphology from SAXS Study. Conventionally, interlamellar segregation can be revealed from a swelling in amorphous layer upon blending, which is manifested by a monotonic increase of l_a with diluent composition. This approach is actually based on the principle that, in the presence of interlamellar segregation, the linear crystallinity must continuously drop with increasing diluent composition. For a full interlamellar segregation, the blend is homogeneously filled with lamellar stacks, thus $\phi_s = 1$ or $\phi_c^{lin} = \phi_c$. Since ϕ_c must drop monotonically with w_{PVC}, interlamellar segregation is characterized by the depression of ϕ_c^{lin} with w_{PVC}; according to eq 6, when l_c is not perturbed by blending, then l_a must rise with w_{PVC} to be consistent with a depression of ϕ_c^{lin} and hence interlamellar segregation. This is the basis for the conventional identification of interlamellar segregation.

On the other hand, for a special case where a depression of crystal thickness occurred upon blending, as encountered in Figure 4b, then according to eq 6, l_a can either increase, decrease, or remain constant for interlamellar segregation, because all three may lead to depression of ϕ_c^{lin} with w_{PVC}. Since l_a drops with w_{PVC}, the presence of interlamellar segregation cannot be identified directly from the composition variations of l_a in Figure 4b.

An alternative approach of identifying the morphological pattern is to consider the magnitude of ϕ_s. This approach has been utilized previously by Saito et al.[26]

As has been pointed out, $\phi_s = 1$ means a full interlamellar segregation, whereas $\phi_s < 1$ denotes the presence of extralamellar segregation. Figure 6 plots ϕ_s against w_{PVC} for the blends with different M_{PCL}. Generally, ϕ_s decreases with w_{PVC}, indicating the presence of interfibrillar morphology over the major composition range. This is in accord with the coarsening in spherulitic texture observed by optical microscopy.

From the values of ϕ_s in Table 2, ϕ_s is approximately unity for pure PCL irrespective of M_{PCL}. Deviations of ϕ_s from unity were observed for the blends. For a given composition, ϕ_s is smaller for the blends containing oligomeric PCL, suggesting a higher extent of interfibrillar morphology in the blends with lower M_{PCL}. This is consistent with the microscopic observation which

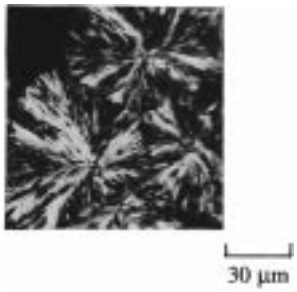

Figure 7. Interfibrillar morphology of pure PCL (M_{PCL} = 1000). It can be seen that even pure PCL can exhibit interfibrillar morphology due to the segregation of uncrystallizable short chains into the interfibrillar regions.

showed more opened spherulites in oligomeric PCL blends.

(C) Determination of Extent of Interfibrillar Segregation for PVC. Table 2 and the microscopic observation in Figure 3 manifest an increasing extent of interfibrillar segregation with decreasing M_{PCL}. Does this mean the transport of PVC into interfibrillar regions was facilitated by lowering the MW of PCL? The answer would be "yes" if PVC was the only component expelled during crystallization. In a previous study, we found that the segregation of uncrystallizable PCL short chains may also lead to interfibrillar morphology in pure PCL oligomers.[19] An example is demonstrated in Figure 7 for PCL with $M_{PCL} = 1000$, where this oligomeric PCL displays quite clear branches within the spherulites. Therefore, two possibilities giving rise to interfibrillar morphology must be considered for the blends containing oligomeric PCL, namely, the rejection of PVC and the segregation of uncrystallizable short chains of PCL. The appearance of compact spherulites in pure PCL oligomer (as that displayed in parts c and d of Figure 3) does not ensure that the observed interfibrillar segregation in the corresponding blends arises solely from the rejection of PVC. For pure PCL, the uncrystallizable short chains may only account for a small portion such that their rejections to interfibrillar zones is not resolved by optical microscopy. On the other hand, if blending reduces the crystallizability by raising the amount of uncrystallizable short chains, these short chains may account for a sufficient portion that their exclusions to interfibrillar regions become resolvable optically. Thus, it is necessary to examine whether the content of uncrystallizable short chains was raised by blending, so that these additional materials may also contribute to the observed interfibrillar morphology.

To evaluate the effect of blending on the content of uncrystallizable short chains, the crystallizability of PCL in the blends is compared with that in pure homopolymer, as demonstrated in Figure 8. The crystallinity presented in Figure 8 was determined from the enthalpy of melting, $\Delta h_f/(\Delta h_f^0 w_{PCL})$, by taking the bulk enthalpy of melting $\Delta h_f^0 = 166.7$ J/g. Division by the weight fraction of PCL, w_{PCL}, is to express the crystallinity in terms of the weight of crystals per unit weight of PCL. The crystallizability of PCL in the blends with $M_{PCL} = 34\,800$ is essentially unaffected, and for the blends with $M_{PCL} = 15\,800$ the crystallizability is slightly depressed. A much stronger depression is observed for the blends with $M_{PCL} = 1200$.

To interpret the strong depression of crystallizability in oligomeric blends, we consider two primary effects that may influence the crystallizability upon blending.

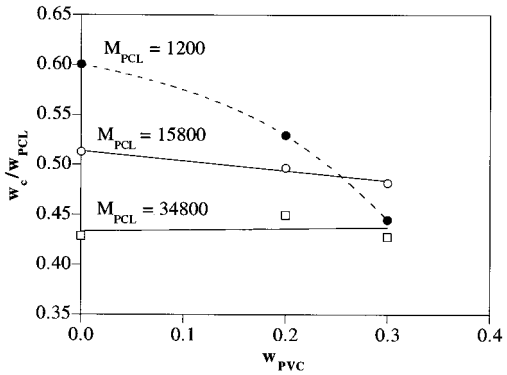

Figure 8. Effect of blending with PVC on the crystallizability of PCL. For the blends with low M_{PCL} (=1200) the crystallizability clearly drops upon blending. For the blends with high M_{PCL}, crystallizability is essentially unaffected.

The first is associated with increased content of uncrystallizable short chains due to the depression of equilibrium melting point (mp). Polymer chains become uncrystallizable above the equilibrium mp and the crystallization proceeds with a negligible rate as the crystallization temperature (T_c) was close to equilibrium mp. Depression in the equilibrium mp upon blending raises the fraction of short chains whose mp is below T_c or close to T_c. As a result, the crystallizability drops. This effect is particularly important for blends containing a crystallizable oligomeric component. The second effect contributing to lower crystallizability is associated with mobility reduction of the crystallizable chains. This effect is particularly important for blends containing crystallizable component with high MW and the blending counterpart has a higher T_g. Reduction in chain mobility could prohibit a portion of the longer chains from crystallizing. In the case of PCL/PVC blends containing oligomeric PCL (e.g. $M_{PCL} = 1200$), the first effect must dominate over the second, since if the second effect were more important, the blends with $M_{PCL} = 34\,800$ should have displayed the strongest depression in crystallizability. Therefore, for the blends with $M_{PCL} = 1200$, the crystallizability of PCL was depressed upon blending due to an increase in the amount of uncrystallizable short chains.

Since the content of uncrystallizable short chains rose in oligomeric blends, these additional PCL short chains may also be expelled to the interfibrillar regions and thus contribute to the observed the interfibrillar morphology. From the viewpoint of molecular mobility, the rejection of PCL short chains into interfibrillar regions should be more favorable than that of PVC molecules. As center-of-mass diffusion is involved in the segregation process, to a first order of approximation, the center-of-mass diffusion coefficient is expressed as $D_{CM} \approx D_0/M^2$ with D_0 being the monomeric diffusion coefficient and M the molecular weight;[27] PCL has a larger D_0 than PVC due to a much lower T_g, and M of short PCL chains is much lower than that of the PVC sample used here ($M_{PVC} = 39\,800$). As a result, D_{CM} of short PCL chains should be larger than that of PVC. It is not unexpected that the rejection of these short chains into interfibrillar regions is more favorable than the exclusion of PVC. The interfibrillar regions in the blends containing oligomeric PCL should thus consist of both PVC and short PCL chains which became uncrystallizable after blending. The crystallizabilities of PCL in the blends with $M_{PCL} = 34\,800$ and 15 800

were hardly affected by blending, the materials residing in the interfibrillar zones must predominantly be PVC molecules.

Since PCL short chains also contribute to the interfibrillar morphology, ϕ_s cannot be used directly for presenting the extent of PVC segregated interfibrillarly. It is possible to deduce the overall volume fraction of PVC residing in the interfibrillar zones. Consider the linear crystallinity, which can be rewritten as

$$\phi_c^{\,lin} = \frac{V_c}{(V_c + V_{PCL}^{\,a,IL} + V_{PVC}^{\,IL})} \tag{8}$$

where V_c is the volume of crystal, $V_{PCL}^{\,a,IL}$ is the volume occupied by amorphous PCL segments in the interlamellar zones, and $V_{PVC}^{\,IL}$ is the volume occupied by PVC in the interlamellar zones. The bulk crystallinity is given by

$$\phi_c = \frac{V_c}{V} \tag{9}$$

Dividing eq 9 by eq 8 to yield ϕ_s as

$$\begin{aligned}\phi_s &= \frac{(V_c + V_{PCL}^{\,a,IL} + V_{PVC}^{\,IL})}{V} \\ &= \frac{(V - V_{PCL}^{\,a,IF} + V_{PVC}^{\,IF})}{V} \\ &= 1 - \phi_{PCL}^{\,a,IF} - \phi_{PVC}^{\,IF}\end{aligned} \tag{10}$$

where $\phi_{PCL}^{\,a,IF}$ is the volume fraction of the PCL short chains in the interfibrillar regions and $\phi_{PVC}^{\,IF}$ is the volume fraction of PVC in the interfibrillar regions. If $\phi_{PCL}^{\,a,IF}$ is known, the volume fraction of PVC expelled into the interfibrillar regions may be calculated. Assuming all PCL short chains that became uncrystallizable after blending were expelled to the interfibrillar regions, $\phi_{PCL}^{\,a,IF}$ is then given by the difference in crystallizability between pure PCL and PCL in the blends with the same MW, namely

$$\phi_{PCL}^{\,a,IF} = (w_c^{\,0} w_{PCL} - w_c)\left(\frac{\rho}{\rho_{PCL}^{\,a}}\right) \tag{11}$$

where $w_c^{\,0}$ and w_c are the weight crystallinities of pure PCL and blend, respectively, and ρ and $\rho_{PCL}^{\,a}$ are the densities of blend and amorphous PCL, respectively. Assuming $(\rho/\rho_{PCL}^{\,a}) \approx 1$ and substituting eq 11 into eq 10, $\phi_{PVC}^{\,IF}$ is given by

$$\phi_{PVC}^{\,IF} \cong 1 - \phi_s - (w_c^{\,0} w_{PCL} - w_c) \tag{12}$$

Figure 9 shows the variation of $\phi_{PVC}^{\,IF}$ with M_{PCL}. Different M_{PCL} dependences are observed. PCL/PVC 80/20 blend exhibits a drop of $\phi_{PVC}^{\,IF}$ with increasing M_{PCL}; with increasing M_{PCL}, the exclusion of PVC transforms from interfibrillar segregation to predominant interlamellar segregation for 80/20 blend. For the other two compositions, interfibrillar segregations of PVC are observed over the MW range, and the extent of PVC expelled interfibrillarly is relatively independent of M_{PCL}.

(D) Interpretation of the MW Dependence of Segregation Behavior. From Figure 9, the effect of

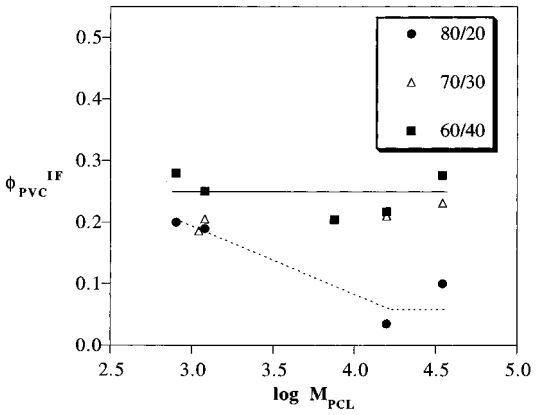

Figure 9. Effect of M_{PCL} on the volume fraction of PVC segregated interfibrillarly ($\phi_{PVC}^{\,IF}$). $\phi_{PVC}^{\,IF}$ drops with increasing M_{PCL} for 80/20 blend, while it is relatively independent of M_{PCL} for the 70/30 and 60/40 blends.

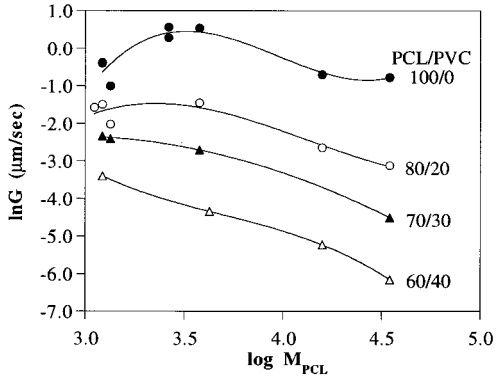

Figure 10. Variations of crystal growth rate (G) with M_{PCL}. The G vs M_{PCL} curve exhibits a maximum for PCL and 80/20 blend, whereas G decreases monotonically with increasing M_{PCL} for 70/30 and 60/40 blend.

M_{PCL} on the segregation distance of PVC is established. For 80/20 blend, the segregation distance of PVC is shortened by increasing the MW of PCL, but such a behavior is absent for the 70/30 and 60/40 blends. The observed M_{PCL} dependence may be interpreted by considering the segregation parameter, $\delta = D/G$. M_{PCL} can affect both D and G and consequently the segregation distance, δ. The diffusion coefficient, D, is related to the center-of-mass diffusion of PVC molecules in the segregation process. The nature of this diffusion coefficient is not established at current stage, while it may be mutual diffusion or self-diffusion depending on the detailed diffusion mechanism involved in the segregation process. Nevertheless, because the motion of polymer molecules in the melt is cooperative, D of PVC is dependent on the MW of the surrounding matrix. The center-of-mass diffusion coefficient of a chain decreases with increasing matrix molecular weight.[28] Thus, D should be reduced by increasing M_{PCL}. As to the change of G with M_{PCL}, G was measured directly by optical microscopy. Figure 10 plots the growth rate against logarithmic M_{PCL}. A maximum in the G vs M_{PCL} curve is identified for pure PCL and 80/20 blend, although the maximum is shallower for the 80/20 blend. Such a maximum is due to the interplay between the thermodynamic driving force and the mobility associated with crystallization.[19] For 70/30 and 60/40 blends, the maximum disappears and the growth rates drop monotonically with M_{PCL}.

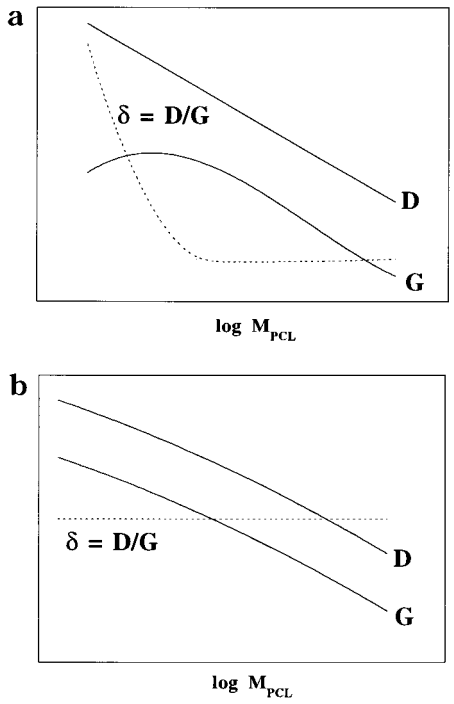

Figure 11. Schematic presentation for the effects of M_{PCL} on D and G and consequently on the segregation distance, $\delta = D/G$, for (a) 80/20 blend which exhibits a maximum in G vs M_{PCL} curve and (b) 70/30 and 60/40 blends which exhibit monotonic drops of G with M_{PCL}. For 80/20 blend, the segregation distance rises with decreasing M_{PCL} at the low M_{PCL} regime because of different M_{PCL} dependences for D and G. For 70/30 and 60/40 blend, the segregation distance may be relatively independent of M_{PCL} since both D and G drop with M_{PCL}.

Figure 11 schematically illustrates the influence of M_{PCL} on the magnitude of δ deduced from the variations of D and G. For 80/20 blend (Figure 11a), D decreases monotonically with M_{PCL} but G shows a maximum. At the low M_{PCL} regime, D and G exhibit different M_{PCL} dependences. The consequence is that the ratio of D/G, or the distance of segregation of PVC, rises with decreasing M_{PCL} under the low M_{PCL} regime. On the other hand, both D and G drop monotonically with M_{PCL} for 70/30 and 60/40 blend (Figure 11b); the consequence is that the ratio of D and G and hence the segregation distance may be relatively independent of M_{PCL}. The interpretation proposed here suggests that the variation of growth rate with M_{PCL} plays the key role in controlling the segregation distance of PVC.

2. Effect of PVC Molecular Weight. Figure 12 shows the spherulite morphologies of PCL/PVC 70/30 blends with M_{PVC} as the variable while M_{PCL} is fixed as 43 700. The spherulite morphology also varies with M_{PVC}, where the banded pattern was gradually disrupted and the spherulite texture becomes more open with decreasing M_{PVC}. This observation suggests that the extent of interfibrillar segregation increases with decreasing M_{PVC}.

As has been indicated in the foregoing discussion that interfibrillar segregation may also arise from the exclusion of short PCL chains which became uncrystallizable upon blending. It seems unlikely that such a contribution is significant in the present systems because of the high MW of PCL ($M_{PCL} = 43\,700$). Figure 13 evaluates the effect of M_{PVC} on the crystallizability of PCL in 70/30 blends. The horizontal dashed line specifies the crystallinity of pure PCL. The crystallizability of PCL

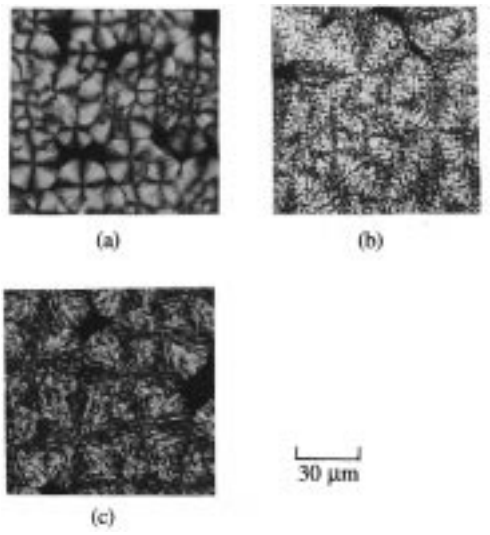

Figure 12. Spherulite morphologies of PCL/PVC 70/30 blends with various M_{PVC}. MW of PCL was fixed as $M_n = 43\,700$. The MW of PVC: (a) 59 700; (b) 25 500; (c) 7200.

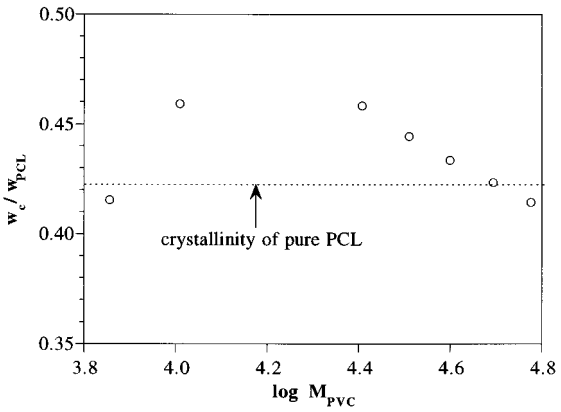

Figure 13. Effect of M_{PVC} on the crystallizability of PCL in PCL/PVC 70/30 blends. The horizontal dashed line specifies the crystallinity of pure PCL.

is not affected significantly by M_{PVC} (the largest perturbation is only 4%). This means that the interfibrillar segregation observed in Figure 12 must be predominantly associated with the exclusion of PVC molecules into the interfibrillar regions.

Figure 14a displays the variations of L, l_c, and l_a with M_{PVC}. The crystal thickness drops slightly with increasing M_{PVC} while the amorphous layer thickness and long period rise with increasing M_{PVC}. The rise of l_a is actually an indication of a greater extent of interlamellar morphology for blend with higher M_{PVC}.

Figure 14b plots the volume fraction of lamellar stacks, ϕ_s, against logarithmic M_{PVC}. ϕ_s increases with increasing M_{PVC}, showing that the extent of interfibrillar segregation drops with increasing M_{PVC}. This is consistent with microscopic observation. If the interfibrillar regions contain predominantly PVC, then the volume fraction of PVC expelled into the interfibrillar zones is simply given by

$$\phi_{PVC}^{IF} \approx 1 - \phi_s \tag{13}$$

Figure 14b also plots ϕ_{PVC}^{IF} as a function of M_{PVC}. As expected ϕ_{PVC}^{IF} drops with M_{PVC}.

The results presented have suggested that the segregation distance of PVC was increased by lowering its

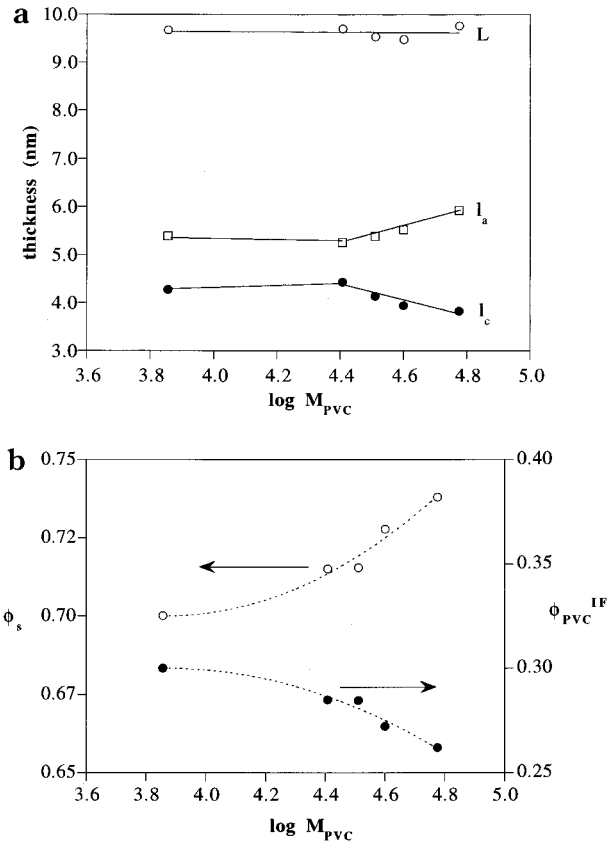

Figure 14. (a) Variations of L, l_c, and l_a with M_{PVC} for PCL/PVC 70/30 blend. (b) Effects of M_{PVC} on the volume fraction of lamellar stacks (ϕ_s) and the volume fraction of PVC segregated interfibrillarly (ϕ_{PVC}^{IF}). The blend composition is PCL/PVC 70/30.

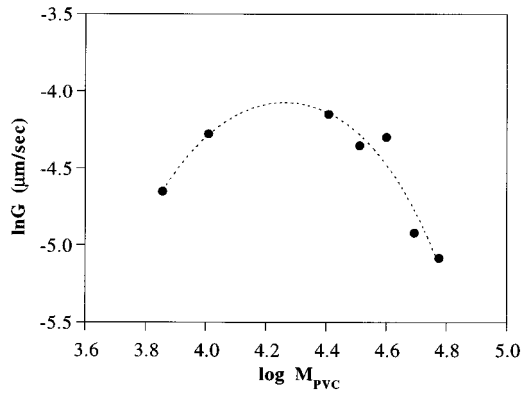

Figure 15. Variation of crystal growth rate (G) with M_{PVC} for 70/30 blend. The G vs M_{PVC} curve exhibits a maximum due to the interplay between thermodynamic driving force and segmental mobility associated with crystallization.

MW. This observation can also be interpreted by the δ parameter. The diffusion coefficient of PVC must of course drop with increasing M_{PVC}. The dependence of growth rate on M_{PVC} for 70/30 blend is shown in Figure 15. Interestingly, the variation of growth rate displays a maximum. The presence of maximum is again attributed to the interplay between thermodynamic driving force and chain mobility associated with crystallization. At the low M_{PVC} regime, depression in equilibrium mp upon blending controls the growth rate. The higher entropy of mixing in the blends with lower M_{PVC} leads to a stronger depression in equilibrium mp and hence the driving force of crystallization; as a consequence, growth rate decreases with decreasing M_{PVC}. Because the variation of growth rate with M_{PVC} also shows a maximum, the effect of M_{PVC} on the magnitude of δ can be similarly depicted in Figure 11a, which prescribes a rise of δ with decreasing M_{PVC}.

The present morphological investigation has suggested that the MW variation of growth rate is the key factor in controlling the segregation distance of the amorphous diluent. This conclusion appears to agree with the study by Runt et al. which emphasized the importance of growth rate on the formation of segregation morphology.[18]

Conclusions

Effects of MW of PCL and PVC on the segregation morphology of their binary blends have been evaluated. The transport of PVC into interfibrillar regions was facilitated by decreasing M_{PCL} for the PCL/PVC 80/20 blend. On the other hand, the extent of PVC expelled interfibrillarly was unaffected by M_{PCL} for 70/30 and 60/40 blends. As to the effect of M_{PVC}, the segregation distance of PVC was found to be reduced by increasing M_{PVC}. The MW variation of growth rate is suggested to dominate the segregation distance of PVC. In the blends where the growth rate exhibited a maximum in its variation with MW, the segregation distance of PVC rises with decreasing MW at the low MW regime because G and D have different MW dependences. The segregation distance is relatively independent of MW for the blends which did not display a maximum in the G vs MW curve. This is because that both G and D drop with MW and their ratio may become relatively insensitive to MW. The results presented in this study suggest that the growth rate and the factors that influence it may dominate the length scale of diluent segregation. Hence, the segregation morphology is expected to depend on crystallization temperature, as the variation of growth rate with temperature is known to display a maximum, while the diffusion coefficient rises monotonically with temperature.

Acknowledgment. We are deeply grateful for Mr. Wen-Jun Liu of the Department of Engineering and System Science at NTHU for his assistance in SAXS experiment. This research is supported by the National Science Council of R.O.C.

References and Notes

(1) Stein, R. S.; Khambatta, F. B.; Warner, F. P.; Russell, T.; Escala, A.; Balizer, E. *J. Polym. Sci., Polym. Symp.* **1978**, *63*, 313.
(2) Defieuw, G.; Groeninckx, G.; Reynaers, H. *Polym. Commun.* **1989**, *30*, 267.
(3) Defieuw, G.; Groeninckx, G.; Reynaers, H. *Polymer* **1989**, *30*, 595.
(4) Hudson, S. D.; Davis, D. D.; Lovinger, A. J. *Macromolecules* **1992**, *25*, 1759.
(5) Huo, P. P.; Cebe, P.; Capel, M. *Macromolecules* **1993**, *26*, 4275.
(6) Sauer, B. B.; Hsiao, B. S. *J. Polym. Sci., Polym. Phys. Ed.* **1993**, *31*, 901.
(7) Russell, T. P.; Ito, H.; Wignall, G. D. *Macromolecules* **1988**, *21*, 1703.
(8) Keith, H. D.; Padden, F. J. *J. Appl. Phys.* **1975**, *35*, 1270.
(9) Khambatta, F. B.; Warner, F.; Russell, T.; Stein, R. S. *J. Polym. Sci., Polym. Phys. Ed.* **1976**, *14*, 1391.
(10) Ong, C. J.; Price, F. P. *J. Polym. Sci., Polym. Symp.* **1978**, *63*, 45.
(11) Russell, T. P.; Stein, R. S. *J. Polym. Sci., Polym. Phys. Ed.* **1983**, *21*, 999.
(12) Morra, B. S.; Stein, R. S. *Polym. Eng. Sci.* **1984**, *24*, 311.

(13) Silvestre, C.; Cimmino, S.; Martuscelli, E.; Karasz, F. E.; MacKnight, W. J. *Polymer* **1987**, *28*, 1190.
(14) Defieuw, G.; Groeninckx, G.; Reynaers, H. *Polymer* **1989**, *30*, 2158.
(15) Defieuw, G.; Groeninckx, G.; Reynaers, H. *Polymer* **1989**, *30*, 2164.
(16) Cheung, Y. W.; Stein, R. S.; Wignall, G. D.; Yang, H. E. *Macromolecules* **1993**, *26*, 5365.
(17) Cheung, Y. W.; Stein, R. S. *Macromolecules* **1994**, *27*, 2512.
(18) Talibuddin, S.; Wu, L.; Runt, J.; Lin, J. S. *Macromolecules* **1996**, *29*, 7527.
(19) Chen, H.-L.; Li, L.-J.; Ou-Yang, W.-C.; Hwang, J. C.; Wong, W.-Y. *Macromolecules* **1997**, *30*, 1718.
(20) Strobl, G. R.; Schneider, M. *J. Polym. Sci., Polym. Phys. Ed.* **1980**, *18*, 1343.
(21) Debye, P.; Bueche, A. M. *J. Appl. Phys.* **1949**, *20*, 518.
(22) Debye, P.; Anderson Jr., H. R.; Brumberger, H. *J. Appl. Phys.* **1957**, *28*, 679.
(23) Ruland, W. J. *J. Appl. Crystallogr.* **1971**, *4*, 70.
(24) Santa Cruz, C. S.; Stribeck, N.; Zahmann, H. G.; Baltá Calleja, F. J. *Macromolecules* **1991**, *24*, 5980.
(25) Albrecht, T.; Strobl, G. *Macromolecules* **1996**, *29*, 783.
(26) Saito, H.; Stuhn, B. *Macromolecules* **1994,** *27*, 216.
(27) de Gennes, P.-G. *Scaling Concepts in Polymer Physics*; Cornell University Press: Ithaca, NY, 1979.
(28) Skolnick, J.; Yaris, R.; Kolinsk, A. *J. Chem. Phys.* **1988**, *88*, 1407.

MA9715740